Universal Growth of Microdomains and Gelation Transition in Agar Hydrogels

Shilpi Boral, Anita Saxena, and H. B. Bohidar*

Polymer and Biophysics Laboratory, School of Physical Sciences, Jawaharlal Nehru University, New Delhi-110 067, India

Received: October 19, 2007; In Final Form: January 12, 2008

Investigations were carried out on aqueous sols and gels of agar (extracted from red seaweed *Gelidiella acerosa*) to explore the growth of microdomains en route to gelation. Isothermal frequency sweep studies on gel samples revealed master plots showing power-law dependence of gel elastic modulus, $|G^*|$, on oscillation frequency, ω as $|G^*| \approx \omega^n$, independent of temperature, with $0.5 \leq n \leq 1.4$. Dynamic structure factor data from sol samples comprised of a double-exponential relaxation function, $S(q,t) = A \exp(-D_S q^2 t) + B \exp(-D_L q^2 t)$ where D_S and D_L are the two translational diffusion coefficients and q is the scattering wave vector. This yielded hydrodynamic radii (from D_S), with R_S varying from ∼20 nm (for sol) to 250 nm (at gelation point). The second hydrodynamic radius (from D_L) obtained was R_L in the range of ∼200−500 nm (for sol) to ∼1000 nm (at 38 °C, gelation point). These data could be universally fitted to $R_S \approx \epsilon^{-3/5}$ and $R_L \approx \epsilon^{-1/3}$ ($\epsilon = (T/T_g - 1)$, $T > T_g$). The $S(q,t)$ behavior close to the gel transition point ($T_g \approx (38 \pm 3$ °C determined from rheology) followed a stretched exponential function: $S(t) = A \exp(-t/t_s)^\beta$. The β factor increased from 0.25 to 1 as the gel temperature approached 25 °C from T_g, and relaxation time, t_s, showed a peak at $T \approx$ 30 °C. The SLS data (in the sol state) suggested the scaling of scattered intensity, $I_s(q) \approx \epsilon^{-\gamma}$ ($\epsilon = (T/T_g - 1)$, $T > T_g$) with $\gamma = 0.13 \pm 0.03$, and the presence of two distinct domains characterized by a Guinier regime (low q) and a power-law regime (high q). Close to and above T_g (+2 °C), $I_S(q)$ scaled with q as $I_s(q) \approx q^{-\alpha}$ with $\alpha = 2.2 \pm 0.2$, which decreased to 1.4 ± 1 just below T_g (−2 °C), implying a coil−helix transition for 0.2% (w/v) and 0.3% (w/v) samples. For a 0.01% sample, $\alpha = 3.5 \pm 0.5$ which indicated the presence of spherical microgels.

I. Introduction

Polymer gels constitute a special class of soft matter as far as their supramolecular structure and viscoelastic properties are concerned. A gel can be defined as a three-dimensional interconnected mechanically percolating structure with the continuous phase (solvent) interacting synergistically with the network.[1] The dispersed phase (polymer) is often found to be present in a disordered and non-ergodic state.[2] Thus, sol−gel transition constitutes a phase change from an ergodic to a non-ergodic state. Biopolymers undergo gelation transition following two signature routes: nucleation and growth and/or spinodal decomposition.[3] Agar and its derivative gels[4,5] have acquired immense interest due to their application potential. Agar is routinely used as a substrate in growing microbial colonies and cells and tissues. These gels can support cartilage phenotype, a concept used in tissue engineering for cartilage repair.[6] The recent fascinating applications of this biopolymer in the construction of a polyelectrolyte diode,[7] and as an aqueous binder in powder injection moulding,[8] have extended its potential tremendously.

Agar comprises mainly of alternating β-(1−4)-D- and α-(1−4)-L-linked galactose residues in a way that most of the α-(1−4) residues are modified by the presence of a 3,6-anhydro bridge.[9] Other modifications commonly observed are mainly substitutes of sulfate, pyruvate, urinate, or methoxyl groups. The gelation temperature of agar is primarily decided by the methoxy content of the sample. Agar sols form thermoreversible physical gels with large hysteresis between melting ($T_m \approx 85$ °C) and gelling ($T_g \approx 40$ °C) temperatures with the constituent unit being antisymmetric double helices.[10,11] Agar gels exhibit syneresis, which is manifested in the continuous evolution of the internal structure. This generates interesting internal relaxation dynamics and an array of characteristic length scales. It has been reported that this sol−gel transition is governed by spinodal decomposition, the double-helix content, and their spatial packing being dependent on agar concentration in the sol.[10] Three distinct stages could be observed during the sol−gel transition that contributes to the evolution of agarose gel topology: (i) induction stage, (ii) gelation stage, and (iii) pseudo-equilibrium stage.[11] Fluorescence correlation spectroscopy (FCS) and small-angle neutron-scattering experiments performed on agarose gels revealed: (i) pore size distribution in the gel phase (size range 1−900 nm), (ii) the existence of supramolecular structures comprising of cylindrical fiber bundles, and (iii) the solute diffusion is considerably hindered by presence of these structures inside the gel phase.[12,13] Gelling properties of alkali-modified agar was investigated by ^{1}H and ^{13}C NMR, and it was found that the gel rigidity and syneresis index could be tailored by the addition of Na^+, K^+, and Ca^{2+} ions.[14] Interestingly, the ion-driven gelation and sulfate location phenomenon observed in these studies conferred agar's similarity to another polysaccharide, κ-carrageenan. Similarly, the melting and gelling temperatures of agar gels were found to decrease significantly in the presence of ionic surfactants, whereas nonionic surfactants had the opposite effect.[15]

The gelatin kinetics and domain growth in agar gels has been explored by some workers in the past.[11,16−19] Simultaneous

* To whom correspondence should be addressed. E-mail: bohi0700@mail.jnu.ac.in. Fax: +91-11-2671-7537 and +91-11-2671-7562.

10.1021/jp7101463 CCC: $40.75
Published on Web 03/01/2008

development of self-similar structures of cross-linked molecules and formation of large scale domains due to spinodal demixing has been reported.[19,20] These two domains undergo kinetic competition for growth until gelation point is encountered facilitated by multiple path interaction processes in the supramolecular assembly. The structural ordering of fractal aggregates in gelling agarose solutions was exhaustively studied and characterized.[21] It was observed that below gelation temperature aggregation process freezes spatial ordering rapidly. Mechanical scanning probe microscope images clearly showed inhomogeneous structure of agar gels comprising domains of various length scales.[22] The domain size decreased with increase in agar concentration. A hierarchy of length scales has been shown to exist in another biopolymer gel, gelatin.[23] The pertinent questions that arise are: (i) Are there structured domains in the sol state of agar? (ii) How does this change as T_g is approached? (iii) Is there any commonality between the microdomain structures observed in agar sols and their gels? This required the systematic exploration of sol and gel states, both below and above the gelation temperature, which constitutes the objective of this work. We use rheology and static and dynamic laser light scattering (SLS and DLS, respectively) to seek answers to the above-mentioned questions.

II. Materials

Powdered agar was generously supplied by Central Salt and Marine Research Institute, Bhavnagar, India, which was used without further purification. This was extracted from the red seaweed *Gelidiella acerosa* collected from the Gulf of Mannar at the southeast coast of India, employing the method described by Craigie and Leigh.[9] The agar had the following physical properties: gel strength, 100 g/cm^2 (1.5% gel at 20 °C); gelling temperature, $T_g \approx 36$ °C; $T_m \approx 85$ °C. The estimated molecular weight was in the range ~120−150 kD. Agar solutions (0.1, 0.2, and 0.3% w/v) were prepared in an autoclave using deionized water as solvent. The accepted gelling concentration for agar is[9] ~0.1% (w/v). However, this concentration may vary with reference to the concentration of agarose and agaro-pectin present in a given agar sample.[9]

III. Experimental Procedures and Data Analysis

All experiments were performed in the temperature-scanning mode. For sol−gel transition studies, hot solutions of agar were taken in quartz 5-mL cylindrical cells for DLS and SLS experiments and were kept in a preheated (90 °C) sample chamber of the light-scattering equipment. For rheology measurements the hot sol was taken on a preheated peltier plate. Another lot of hot sols was allowed to cool to room temperature and to form optically transparent gels. After 2 days, these gels were assumed to have been stabilized and various experiments were performed. All samples were prepared in duplicates.

(a) Rheology. Rheological measurements using small amplitude oscillatory shear were performed on the agar gels using controlled stress AR 500 rheometer (TA Instruments, Surrey, England). For all tests, the storage and loss modulus (G' and G'') were computed from raw oscillatory data using TA Instrument Rheology Advantage Data Analysis software (version 3.0.1). All measurements were performed in duplicate with highly reproducible data (relative standard deviation less 5%) for each sample. The rheological studies were carried out in two independent sets of experiments that comprised temperature and frequency sweep measurements. We have preferred to use the dynamic modulus $|G^*|$ instead of G' or G'' because the $|G^*|$ data was found to be more systematic and had less fluctuations.

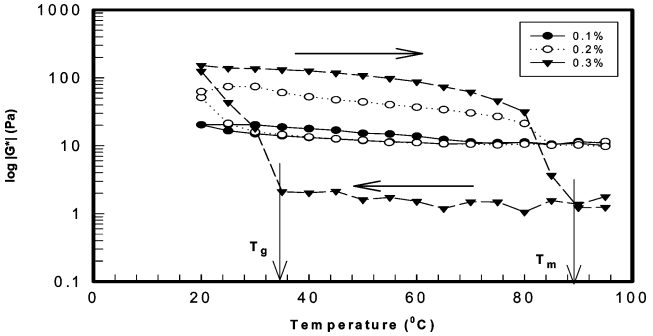

Figure 1. Isochronal temperature-sweep data taken on agar system. The heating and cooling rate was 5 °C/min. The determination of T_g and T_m could be achieved without ambiguity.

Rheological behavior of the samples close to, and above and below, the sol−gel transition region was probed by performing isochronal temperature sweep experiments using cone-plate geometry (2-cm diameter, 2° cone angle, and 56-mm gap). The hot sols were loaded onto the preheated peltier plate (95 °C) of the rheometer and allowed to equilibrate for 5 min. The periphery of the geometry was coated with light silicon oil and enclosed within a wet sponge supplied by the manufacturer in order to minimize solvent evaporation. Temperature dependence of dynamic modulus $|G^*|$ was recorded by cooling the systems from 95 to 20 °C at the rate of 5 °C/min and then reheating to 95 °C at the same rate to complete the thermal cycle. The angular frequency was fixed at 6.2830 Hz, and controlled stress was 4.7750 Pa. The gel and melting temperatures (T_g and T_m) were determined from the abrupt change in slope of the cooling and heating cycles data, which is clearly shown in Figure 1.

The 2-day-old agar gel samples of different concentrations were loaded onto the rheometer plate preheated to different temperatures ranging from 25 to 45 °C to generate data shown in Figure 2. Measurements were carried out with a cross-hatched parallel plate (2-cm diameter, 58-mm gap) geometry using a constant oscillation stress of 6.3660 Pa. The effect of oscillatory frequency on the dynamic rheological properties of the gel network was evaluated at these temperatures after the gels were allowed to equilibrate for 5 min. The mechanical spectra were characterized by $|G^*|$ as a function of angular frequency in the range of 0.628 to 200 rad/s.

(b) Light Scattering. SLS and DLS experiments were performed (mostly at scattering angle of $\theta = 90°$ and laser wavelength of $\lambda = 632.8$ nm) on a 256-channel Photocor-FC (Photocor Inc., USA) that was operated in the multi-τ mode (logarithmically spaced channels). The time scale spanned 8 decades, i.e., from 0.5 μs to 10s. The samples were housed inside a thermostated bath, and the temperature was regulated by a PID temperature controller to an accuracy of ±0.1 °C. In all the experiments, the difference between the measured and calculated baseline was not allowed to go beyond ±0.1%. The data that showed excessive baseline difference were rejected. The probe length scale is defined by the inverse of the modulus of the scattering wave vector q where the wave vector $q = (4\pi\mu/\lambda)\sin(\theta/2)$, and the medium refractive index is μ. The measured intensity autocorrelation data were manually fitted to user defined multiexponential functions. The integrated intensity of scattered light was collected at various temperatures. Robustness of the results was decided based on two criteria: sample-to-sample accuracy and data reproducibility within the same sample. Polymer gels, intrinsically, are non-ergodic, which increases the complexity of data analysis associated with DLS experiments.[24−26] The standard analysis of light-scattering data requires that the system is completely ergodic (means that time

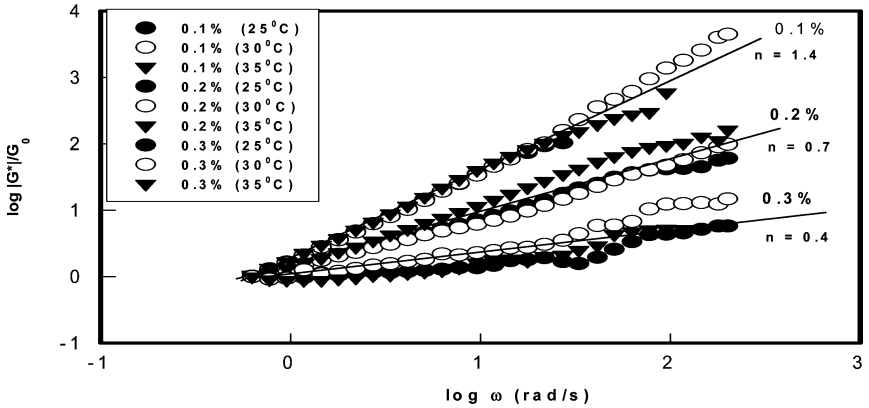

Figure 2. Frequency-sweep studies on agar gel samples as function of sample temperature. G_0 corresponds to the $|G^*|$ value at $\omega = 0.63$ rad/s. A power-law frequency dependence ($|G^*| \approx \omega^n$) is clearly seen with the exponent n decreasing with increasing agar concentration. Data for $T >$ 35 °C was noisy.

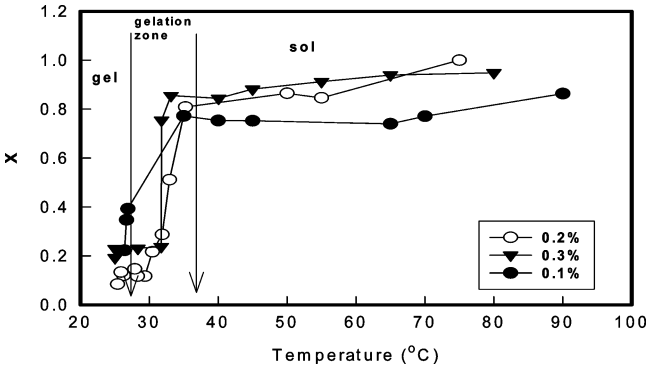

Figure 3. Variation of ergodicity parameter X as a function of sample temperature for gelling agar sols. Notice that closer to T_g (~38 °C) the X value rapidly falls, a trend that continues until the sample temperature reaches 30 °C. This value stabilizes at 0.16 for temperatures less than 30 °C. The temperature window 30−40 °C defines the gelation region.

and ensemble averages are identical) and stationary (process is independent of origin of time), which is adequately satisfied only in case of scattering from dilute solutions. To make the DLS measurements compatible with the said requirements, this problem was addressed in the following way. The normalized intensity correlation function, $g_2(q,t)$, obtained from the gel sample can be related to the dynamic structure factor, $S(q,t)$ as[24,25]

$$g_2(q,t) = 1 + \beta'[2X(1 - X)S(q,t) + X^2|S(q,t)|^2] \quad (1)$$

where β' is the coherence area factor having a maximum value of 1 and defines the signal-to-noise ratio in experiments. The parameter X ($0 \le X \le 1$) defines the ergodicity via the amount of heterodyne contribution present in the correlation data. Thus X accounts for the non-ergodic contribution buried in the measured data in a measurable way. Both β' and X are measurable parameters in a real experiment. The measured intensity autocorrelation data was analyzed exactly following the description given in ref 26. For the gels, we found $X \approx 0.16 \pm 0.04$, independent of gel concentration (see Figure 3). Thus the prefactor of the linear term in $S(q,t)$ in eq 1 is ~20 times larger than the quadratic second term. This gave

$$S(q,t) \approx [g_2(q,t) - 1]/[2\beta'X(1 - X)] \quad (2)$$

Any error thus accrued is absorbed as experimental error in subsequent data analysis. Figure 3 clearly shows that the gel is trapped in a non-ergodic phase after gelation. It is interesting to observe that the X parameter changes gradually in the temperature window ~30−40 °C. Above 40 °C the sample was a clear sol (fully ergodic), and below 30 °C, it had the signature of a non-ergodic gel.

To avoid over dependence on the Laplace inversion method, independently, unsuccessful attempt was made to fit the sol state structure factor data to a single exponential and also to a three exponential relaxation mode (observed in some gels[27]) model with the intermediate mode being a power-law mode. This gave credence to the applicability of a two-mode relaxation process to the $S(q,t)$ data. Having confirmed this all $S(q,t)$ obtained from sols were least-squares fitted to the functional form

$$S(q,t) = A \exp(-D_S q^2 t) + B \exp(-D_L q^2 t) \quad (3)$$

where the two translational diffusivity coefficients are given as D_S and D_L, implying the existence of two distinct particle sizes. Here, A and B are amplitudes of the two relaxation modes. The correlation data was analyzed through user-defined least-squares fitting routines of Sigma Plot software (SPSS, USA). The diffusivity values could be related to corresponding hydrodynamic radii through Stoke−Einstein relation as

$$D_{S,L} = k_B T/(6\pi\eta_0 R_{S,L}) \quad (4)$$

where solvent viscosity is η_0, k_B is Boltzmann's constant, and T is absolute temperature. Here, R_S and R_L correspond to the hydrodynamic radii of small and large particles, respectively. The variation of these values as a function of sample temperature is plotted in Figure 4. In the case of gel samples, the $S(q,t)$ data could be adequately fitted to a stretched exponential function given by

$$S(q,t) = \mathrm{A} \exp -(t/t_s)^{\beta} \quad (5)$$

Here t_s is the relaxation time, and β is width of the distribution function that uniquely characterizes the structure factor $S(q,t)$. A least-squares fitting of the data yielded the t_s and β values, and these are plotted in parts A and B of Figure 5.

The scattering chamber assembly used in our experiments uses an index-matching bath, and the optics is so designed that the direct light is guided out of the scattering chamber that enabled accurate measurement of absolute scattered intensity even at low angles. This integrated scattered intensity was measured as a function of scattering angle and sample temperature for all the three concentrations of agar. The experimental data is shown in Figure 6.

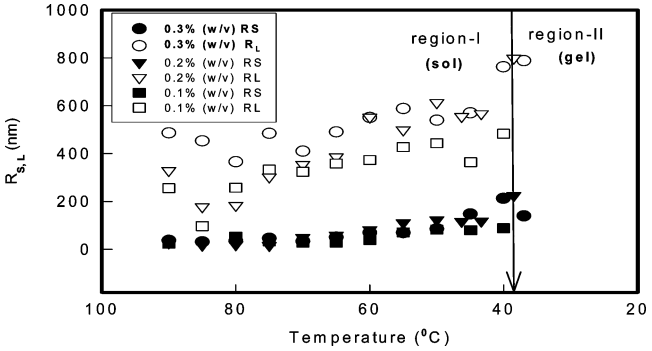

Figure 4. Hydrodynamic radii of scattering moieties seen in gelling agar solution indicating the existence of two distinct sized scattering centers. The larger-sized centers are heterogeneous domains while the smaller particles correspond to the size of low molecular weight components of agar molecule.

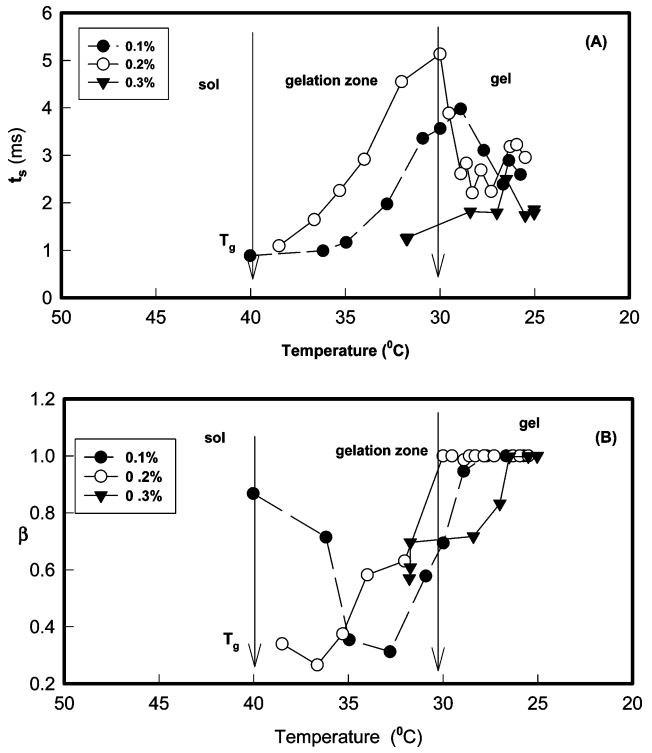

Figure 5. Variation of gel mode relaxation time, t_s, and width parameter, β, as function of temperature for agar hydrogels. Notice that, in the temperature window 30−40 °C, there is an abrupt change in behavior of these parameters. This defines the gelation zone.

IV. Results and Discussions

The experimental results can be discussed distinctively pertaining to the three physical conditions of agar solutions: the transition, sol, and gel phases.

(a) Sol−Gel Transition. The isochronal temperature sweep experiments were performed on the samples to generate the thermal hysteresis loop shown in Figure 1. Two facts are obvious from this data. First, at higher agar concentration the area under the loop tends to be larger, but the 0.1% (w/v) gel showed a very weak hysteresis behavior. Second, the gelation and melting temperatures could be clearly established from the change in slope in the $|G^*|$ data as shown in the figure. The values obtained were $T_g = 38 \pm 2$ °C and $T_m = 85 \pm 5$ °C, independent of agar concentration >0.1% (w/v). The T_g and T_m values obtained are in excellent agreement with the values reported in the literature.[9−11,15−19] For the 0.1% (w/v) sample these temperatures could not be determined without ambiguity. Gel transition behavior could also be captured in our SLS and DLS experiments by conducting measurements in the temperature range 90−25 °C. The intensity vs temperature data are represented in Figure 6, for three the agar concentrations, 0.1, 0.2, and 0.3% (w/v). If one ascertains the T_g value from the data presented in Figure 5, one gets $T_g \approx 38$ °C, a result not too far removed from the same observed by rheology experiments. The melting-phase behavior could not be captured in these experiments. Intensity shows rampant fluctuation in the temperature range ∼30−40 °C though an increasing trend can be unmistakably observed even in this gelation region.

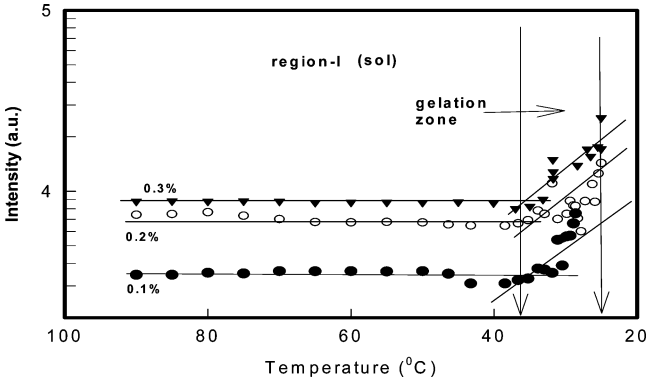

Figure 6. Variation of scattered intensity as a function of temperature of a gelling agar sol taken at a fixed scattering angle of 90 °C. Close to T_g one observes a clear gelation transition characterized by a sharp change increase in the intensity value. Notice the fluctuations in the temperature window 40−30 °C.

The q dependence of scattered intensity $I_S(q)$ was seen to scale with wave vector q as (for $50 < \theta < 140°$)

$$I_S(q) \approx q^{-\alpha} \tag{6}$$

A plot of the ln $I_S(q)$ data as function of ln q at $T \approx (T_g + 2)$ °C, shows a straight line fitting with a slope equal to 2.0−2.4, characteristic of (self-avoiding) Gaussian chain, which decreased to 1.5−1.3 at $T = (T_g - 2)$ °C, characteristic of rod shape for 0.3 and 0.2% samples, confirming a coil−helix transition. Ideally for a stiff helix (assumed to be a rod), the exponent should be 1. Since, we see a drop of almost 100% in the value for α, we argue that a coil to helix type transition is a possibility. The variation of α with temperature is shown in Figure 7, and the inset shows a representative data fitting as predicted by eq 6.

For the 0.1% sample, the corresponding slope was in the range of ∼3.0−3.8, implying conformation in between that of a sphere (4.0) and disc (2.0). This result does not show any coil−helix transition at this concentration, though soft gel was formed at lower temperature, which could be due to formation of nearly spherical microgels connected together. It is widely accepted that the gelation of agarose involves a coil−helix transition of the galactan molecules.[28] The formation of helices and subsequent association of the helices are essential features in the gelation schemes of agarose.[21,29] Bulone et al. have found that $\alpha \approx 3$ independent of quench temperature for agarose gels of concentration 0.5%, a conclusion that agrees with our 0.1% gel data. They argued that the concurrent process of cross linking could interfere with the ripening of domains. The observation of a central peak that moved toward high q values as T_g was approached, and the existence of a self-similar asymptotic tail could be assimilated into a phenomenological model that described the initial growth of aggregates and their subsequent condensation into domains.[21]

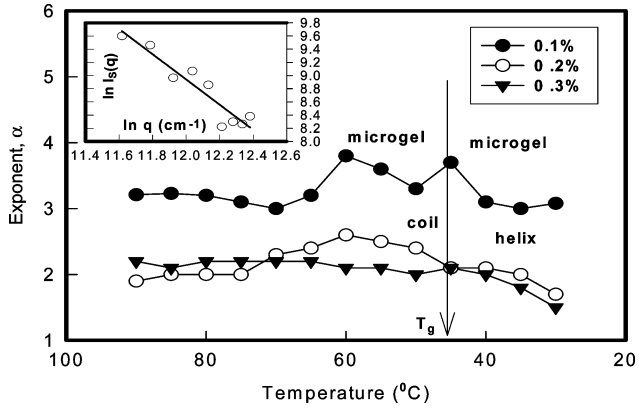

Figure 7. Plot of power-law exponent defined by eq 6, which clearly reveals the change in morphology of the agar molecules in a gelling sol as T_g is approached. Notice that the 0.1% sample retains its morphological integrity even beyond T_g. The other two samples undergo the coil−helix transition. See text for details. Solid lines are to guide the eye.

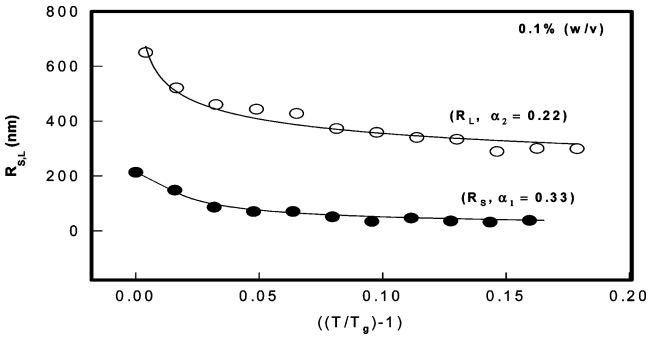

Figure 8. Scaling of R_S and R_L as function of reduced temperature ($T/T_g - 1$) for a 0.1% (w/v) gel that follows the power-law description given by eq 7. Similar results (but with different exponents) were observed for the 0.2 and 0.3% (w/v) samples. See text for details. Solid lines are data-fitted curves.

It is informative to explore how the characteristic size (R_S and R_L) and intensity ($I_S(q)$) of the samples evolved as the gelation point was approached. The size data could be universally fitted to

$$R_S \approx \epsilon^{-\alpha 1} \text{ and } R_L \approx \epsilon^{-\alpha 2} \tag{7}$$

where the reduced temperature $\epsilon = (T/T_g - 1)$, $T > T_g$. A representative plot is shown in Figure 8 for 0.1% (w/v) gel sample that shows $\alpha_1 = 0.33$ and $\alpha_2 = 0.22$. For 0.2 and 0.3% (w/v) samples, we observed $\alpha_1 = 0.6$ and $\alpha_2 = 0.33$. Similarly, the SLS data suggested the scattered intensity to scale with reduced temperature, ϵ, as

$$I_s(q) \approx \epsilon^{-\nu} \tag{8}$$

The plots are shown in Figure 9, and the exponent $\nu = 0.13 \pm 0.3$ for 0.2 and 0.3% (w/v) gels, whereas the 0.1% (w/v) gel yielded a smaller exponent, $\nu = 0.04$. In the critical phase transition picture, a percolating network defined by a characteristic length (called correlation length, ξ, and cluster mass, M, shows

$$M \approx e^{-1.24} \text{ and } \xi \approx \epsilon^{-0.63} \tag{9}$$

The above exponents remain valid for ferromagnets, liquid−gas phase transitions, and binary fluid mixtures. The exponent values pertain to 3-D Ising model predictions.[30,31] The same

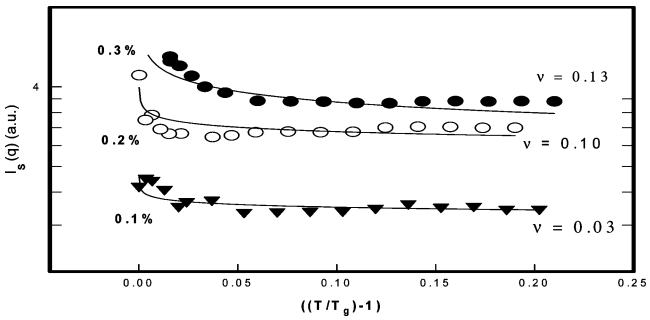

Figure 9. Scaling of scattered intensity as function of reduced temperature ($T/T_g - 1$) for all gel samples that reveals the power-law description given by eq 8. See text for details. Solid lines are data fitted curves.

concept when applied to gelling systems gives[32] $M \approx \epsilon^{-1.8}$. Two observations could be made from this data: (i) behavior of 0.1% (w/v) gel is significantly different from the others; (ii) the sol−gel transition path is not describable through the percolation type of model. However, Tokita and Hikichi[33] studied the sol−gel transition in agarose system and observed that the gelation transition could be explained through the percolating resister network model with the gel elastic modulus, $G \approx |\epsilon|^t$ with $t = 1.93$. This was in agreement with the conductivity exponent[34] of the resister network which predicts $t = 1.98$. It was proposed that in the transition region gel is formed by the tenuous network irrespective of the mechanism of cross-linking formation pathway. On the other hand, the three-stage topology evolution model comprising induction stage, gelation stage, and pseudo-equilibrium stage described by Xiong et al.[11] close to T_g for agarose hydrogels adequately described the experimental data.

Small-angle light-scattering studies yielded aggregates of size ~1−4 μm when the gelation point was approached concomitant with a decrease in the α-value from 3.0 to 2.6, indicating loss of compactness of the aggregates due to domain ripening.[21] Our results increase in aggregate size and fall in α-value from ~2.4 to ~1.4, qualitatively agrees with this observation. Microdomain structures in agar gels have been clearly observed and recorded in mechanical scanning probe microscopy images.[22]

(b) Sol Phase Behavior. For all three concentrations, $S(q,t)$ data in the sol state could be best fitted to a double-exponential function, given by eq 1, yielding two relaxation modes, the first mode arising due to the presence of smaller size particles (R_S = 20−50 nm), which slowly increased to an approximate size ~200 nm as the gelation temperature was approached, and the second mode arising due to the presence of larger or aggregated particles having size in the range ~400−700 nm. A comparative look at Figure 5 revealed that, for $T > 40$ °C, $I_S(q)/C$, where C is agar concentration, remains invariant of the temperature. Recall that $I_S(q)$ can be expressed as[35]

$$I_S(q) = KCMP(q)S(q) \tag{10}$$

where the molecular weight of the scattering moiety is M, $P(q)$ is geometrical form factor, and $S(q)$ is the interparticle structure factor. The sols can be considered to be a dilute and amorphous phase that allows one to assume $S(q) \approx 1$. Thus, the data in the region I of Figure 5 basically comes from M and $P(q)$ contributions implying change in domain (aggregated clusters) size and their geometrical conformations. Size change was captured in DLS experiments. The DLS data (Figure 3) yielded two distinct hydrodynamic radii values, R_S and R_L, as mentioned above. Since the scattered intensity is biased toward the large size particles that were present in all the three samples, their

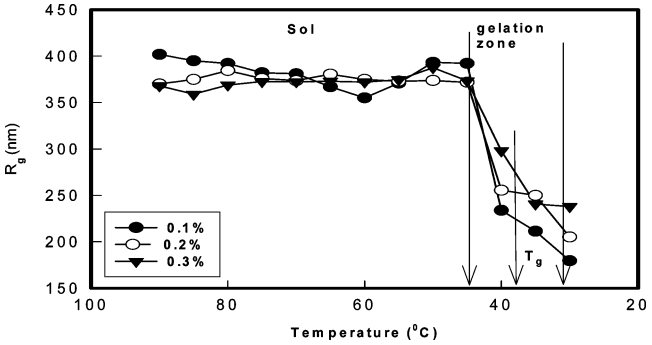

Figure 10. Variation of R_g as function of temperature of a gelling agar sol deduced from Guinier plot defined by eq 11 in the low q values T_g is defined as the midpoint of gelation zone. Solid lines are guide to the eye.

net contribution to $I_S(q)$ would not differ much. This was observed in the sol state data presented in Figure 5.

SLS data as a function of temperature (90−25 °C) and scattering angle (10−40°), corresponding to inverse scattering vectors lying in the range ∼40−450 nm, was examined in the Guinier regime. This data at each temperature suggested the presence of a characteristic length scale, in which an assortment of particles with mean radius of gyration R_g coexist. The Guinier regime could be defined as $R_{gL}q < 1$, and hence

$$I_S(q) \approx I_0 \exp(-R_g^2 q^2/3);\ q < 1.1 \times 10^5\ \mathrm{cm}^{-1} \quad (11)$$

where I_0 is the amplitude and the R_g values obtained were ∼370 ± 15 nm which abruptly dropped to ∼200 nm as T_g is approached. This is shown in Figure 10. In the $q > 1.1 \times 10^5$ cm^{-1} region, we observed a power-law dependence of $I_S(q)$ with q, which has been discussed earlier (eq 6). In Figure 10, T_g is defined as the midpoint of the gelation region.

Sol state characterization of agar has not attracted much attention in the past. Bulone and San Biagio have shown that at very low agarose concentrations (<0.1% w/v) mesoscopic gels can form in polymer-rich domains due to spinodal demixing.[16] DLS studies revealed the presence of elongated agarose structures entangled in a continuously rearranged (transient) mesh with scaling features typical of flexible neutral chains. The values for R_g (above T_g) shown in Figure 10 could well be the size of these mutually disconnected agar helices. Below T_g, these get interconnected, and an effective mesh size having dimension much less than R_g evolves (and probed by DLS) as shown in Figure 10.

(c) Gel Phase Behavior. In the gel phase, intensity rises gradually (see Figure 5) indicating the start of gelation where Brownian motion of the domains slow down due to lowering of temperature, phase separation, and nascent network formation starts.[16−20] The dynamic structure factor, $S(q,t)$, obtained from DLS experiments could be well represented by stretched exponential function defined by eq 3 adequately characterized by a time scale t_S and width parameter β. Both these parameters are plotted as function of temperature in Figure 4. At the start of gelation, β values had been found in between $0 < \beta < 1$ (except for 0.1% gel) showing an increase as T_g was approached, and at around 30 °C, β assumed a value of ∼1 for all three concentrations. Figure 6 indicated coil−helix transition and existence of helical structures in the gel phase. Figure 10 implies collapse of the extended structures of dimension, $R_g \approx 300$ nm into compact domains of size ∼200 nm. Interestingly, the characteristic relaxation time t_s exhibits identical behavior. Both, β and t_s have relatively stable values for $T < 30$ °C and $T > T_g$. This implies that the onset of gelation possibly starts at $T_g = 38$ °C, and the process completes when $T = 30$ °C with the generation of a pseudogel. The internal structure of such a gel undergoes time-dependent evolution due to syneresis. A detailed study of this is underway.

Frequency-sweep studies have been done in oscillatory mode at constant oscillation stress, which provides information about the microstructure of the samples. The frequency range chosen was from very low to very high (0.6283−200.3 rad/s), and experiments were done at three different temperatures of the gel samples below T_g, which is shown in Figure 2. Variation in dynamic modulus $|G^*|$ follows a power-law dependence given by[36]

$$|G^*| \approx S\omega^n \quad (12)$$

where S is a parameter that accounts for the gel strength and ω is the angular frequency. The isothermal frequency sweep studies revealed master plots showing power-law dependence of gel elastic modulus $|G^*|$ on oscillation frequency independent of temperature, with $n = 1.4 \pm 0.02$, 0.7 ± 0.2, and 0.5 ± 0.2 for 0.1, 0.2, and 0.3% (w/v) gel samples, respectively. The gel strength S was found to be same for all samples at ∼30 °C, an observation that indicated that this was the temperature of formation of a pseudogel.

The linear viscoelasticity model, for pre- and postgel situations, proposed by Winter[34] predicts that the stress−relaxation to follow the power-law frequency dependence behavior given by eq 10 with $0 < n < 1$. Stoichiometrically balanced and imbalanced crosslinked networks showed $n = {}^1/_2$ (excess crosslinker) and $n > {}^1/_2$ (lack of crosslinker), respectively. However, this description strictly applies to chemically crosslinked gels, thus the observation of $n > 1$, for the present system where no crosslinker is present per se does not come as a surprise. It was further argued that the crossing of $G'(\omega)$ and $G''(\omega)$ in a small amplitude oscillation shear experiment does not necessarily establish the gelation point. A theoretical rheological model for agar gels was proposed by Labropoulos et al.[37] that assumes temperature dependence of monomeric friction coefficient of agar molecules, which allows net association rate en route to gelation to be estimated from time−temperature data. Rheological measurements, using a dynamic mechanical analyzer, carried out by Chen et al.[38] in the frequency sweep shear sandwich mode (0.1−20 Hz) revealed that $|G^*| \approx \omega^n$ with n ranging between ∼0.025 and 0.035, which allowed the agar gels to be modeled within the fractional derivative frame work. These results indicate that power-law exponent can assume a range of values.

The structure−property studies carried out on equilibrium gels of this biopolymer revealed that the dynamic Young's modulus determined from small deformation rheology could be related to molecular weight of agar.[39−41] The typical viscoelastic length scale prevalent in these materials becomes easily accessible from oscillatory rheology measurements. The viscoelastic length calculated from the measured value of G_0 is plotted in Figure 10 as a function of gel concentration. In a network of connected chains, the shear modulus is proportional to the concentration of intermolecular bonds. The value of the length of elastically active strands is similar to the characteristic viscoelastic network size, ζ_v, estimated from the low-frequency shear modulus, G_0. This gives a qualitative picture of the length over which the viscoelastic stress remains significant. Thus, G_0 is a measure of elastic free energy stored per unit volume of a characteristic viscoelastic network of size, ζ_v. This implies[42]

$$G_0 \approx k_B T/\zeta_v^3 \quad (13)$$

The viscoelastic length values, thus deduced, are plotted in Figure 11. It is interesting to note that in the 0.1% gel sample there is no significant temperature-dependent change in the ζ_v value, implying the microgel nature of this sample. For the two other samples it was clearly seen that ζ_v decreased with increasing polymer concentration indicating the formation of more compact network structures at higher agar concentration.

VI. Conclusions

Agar exhibits a complex gelation mechanism, which has been subjected to intense scrutiny in the past. The sol-to-gel transition involves multiple and characteristic pathways.[20,21,43,44] In the present studies an insight into the gelation mechanism and evolution of microstructures in the sol and gel states of agar was successfully explored. Agar is a mixture of two components: agarose, a neutral polysaccharide, and agaropectin, a charged, sulfated carbohydrate polymer.[9] This chemical structure enables intermolecular interactions through an array of forces: vander Waals forces, hydrogen bonding, and electrostatic interactions. In the gel state the molecules adopt a threefold double-helix conformation.[28,29] The hysteresis loop found in the temperature sweep data (see Figure 1) can be explained on the basis of strength of interaction energy, which is principally related to the proximity of the chains to each other and the number density of hydrogen bonds. While agar chains have a large number of potential hydrogen-bond sites, each water molecule can only form up to four hydrogen bonds. Thus, the inherent strength of the interaction between agar and water is less than that between two agar chains or between two segments of a single agar chain. Therefore while the association between water and agar may be easily broken, the association between two agar molecules is less likely to be disturbed. This leads to very high melting temperature. Second, gelation seems to be a gradual process that is initiated close to $T_g = 38$ °C and ends at 30 °C. Thus, the sol−gel transition in agar system occurs over a temperature window, which is typically 40−30 °C. A pseudogel is formed at 30 °C that structurally evolves with time due to syneresis.

In aqueous solution, however, the existing hydroxyl and sulfate groups in the agar form hydrogen-bonded structures with water, and there is dominant intra- and interchain interaction (in the absence of complexing ions) giving rise to two types of entities, nonassociated and associated agar molecules. This is reflected in the data obtained from DLS measurements (see Figure 4). The sol state is characterized by two sizes of particles, single (20−50 nm) and associated (200−700 nm), both having Gaussian chain (random coil) character. These associated molecules form clusters not interconnected to each other. From SLS and DLS measurement results, the coherent picture of gelation mechanism that emerges is, as the temperature of sol decreases to approach T_g, the hydrodynamic radii of these particles slowly increase up to a temperature ~40 °C with the concomitant loss of their Gaussian character and evolution of rodlike conformations as seen from Figure 7. As soon as the rods are formed, network formation starts giving rise to inhomogenities in the structure and confers stretched exponential behavior to the autocorrelation curves (eq 5) and increase in scattered intensity (Figure 6). Once a network is formed, slow cooperative movement of entangled transient networks of polymer chains starts. The gel network is associated with a characteristic renewal time or the lifetime of the network. The gel network is in dynamic equilibrium with the mesh, which is constantly disturbed and restored over a characteristic time scale.[16,21] The network is initially compliant, thus its contribution to the dynamic moduli of the system include a frequency dependent term. The frequency dependence of the network gradually disappears as more and more agar molecules associate, finally reaching equilibrium moduli values.

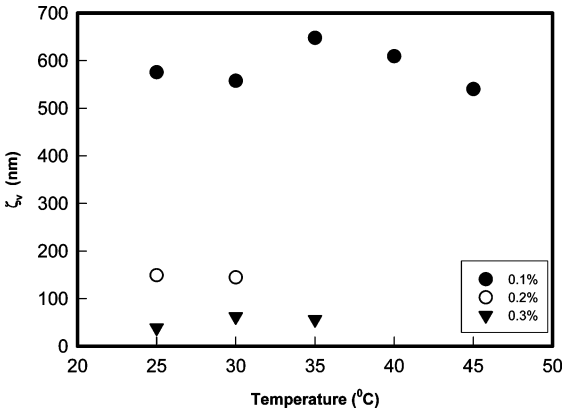

Figure 11. Variation of viscoelastic length as function of temperature of a gelling agar sol deduced from the low-frequency G_0 data (eq 13). The 0.1% gel did not show much temperature-dependent variation, whereas it was significant in the other two high-concentration samples. See text for details.

The self-assembly of agar molecules en route to gelation clearly indicated simultaneous growth of self-similar aggregates and larger macrodomains due to spinodal demixing. Interestingly, it was observed that such microdomains existed even in sol state at temperature far away from T_g. Both these observations are consistent with earlier findings,[16,20] though we established the growth features on a more sound footing. It must be realized that there have not been enough experimental investigations to probe these phenomenon in depth and to establish their universality. The results presented provide a significant insight into the distinctive microstructural features of agar sol that dynamically evolve and form a gel. This paper does not answer all the questions related to the origin and growth of the microdomain structures of such complex systems, yet it makes an attempt to give some foundation to its understanding.

Acknowledgment. We are thankful to the Department of Science Technology (DST), Government of India, for a research grant. A.S. was supported by a Women Scientist Scheme A from the same agency.

References and Notes

(1) Bohidar, H. B.; Dubin, P. L.; Osada, Y. *Polymer Gels: Fundamentals and Applications*; American Chemical Society: Washington DC, 2002; Vol. 833.

(2) Tanaka, H.; Jabbari-Farouji, S.; Meunier, J.; Bonn, D. *Phys. Rev. E* **2005**, *71*, 021402 and **2004**, *69*, 031404.

(3) Strobl, G. *Physics of Polymers*; Springer: Berlin, Germany, 1997.

(4) Norziah, M. H.; Foo, S. L.; Karim, A. A. *Food Hydrocolloids* **2006**, *20*, 204.

(5) Clark, A. H.; Richardson, R. K.; Ross-Murphy, R. K.; Stubbs, J. M. *Macromolecules* **1983**, *16*, 1367.

(6) Cayre, O. J.; Chang, S. T.; Velev, O. D. *J. Am. Chem. Soc.* **2007**, *129*, 10801.

(7) Saris, D. B.; Mukherjee, N.; Berglund, L. J.; Schulz, F. M.; An, K. N.; O'Driscoll, S. W. *Tissue Eng.* **2000**, *65*, 531.

(8) Labropoulos, K. C.; Rangarajan, S.; Niesz, D. E.; Danforth, S. *J. Am. Ceram. Soc.* **2001**, *84*, 1217.

(9) Craigie, J. S.; Leigh, C.; in Hellebust, J. A.; Craigie, J. S. *Hand Book of Phycological Methods*; Cambridge: Cambridge, 1978; p 109.

(10) Pines, E.; Prins, W. *Macromolecules* **1972**, *6*, 888.

(11) Xiong, Jun-Ying.; Narayanan, J.; Liu, Xiang-Yang; Chong, T. K.; Chen. S. B.; Chung, Tai-Shung *J. Phys. Chem. B* **2005**, *109*, 5638.

(12) Fatin-Rouge, N.; Wilkinson, K.; J.; Buffle, J. *J. Phys. Chem. B* **2003**, *107*, 12126.
(13) Fatin-Rouge, N.; Wilkinson, K.; J.; Buffle, J. *J. Phys. Chem. B* **2006**, *110*, 20133.
(14) Villanueva, R.; Montano, N. *J. Appl. Phycology* **1999**, *11*, 225.
(15) Prasad, K.; Siddhanta, A. K.; Rakshit, A. K.; Bhattacharya, A.; Ghosh, P. K. *Int. J. Biol. Macromolecules* **2005**, *35*, 135.
(16) Bulone, D.; San Biagio, P. L. *Biophys. J.* **1995**, *68*, 1569.
(17) San, Biagio, P. L.; Madonia, F.; Newman, J.; Palma, M. U. *Biopolymers* **1986**, *25*, 2255.
(18) San Biagio, P. L.; Bulone, D.; Emanuele, A.; Madonia, F.; Di Stefano, L.; Giacomazza, D.; Trapenese, M.; Palma-Vittorelli, M. B.; Palma, M. U. *Makromol. Chem.* **1990**, *40*, 33.
(19) Feke, G. T.; Prins, W. *Macromolecules* **1974**, *7*, 527.
(20) Manno, M.; Palma, M. U. *Phys. Rev. Lett.* **1997**, *79*, 4286.
(21) Bulone, D.; Giacomazza, D.; Martorana, V.; Newman, J.; San, Biagio, P. L. *Phys. Rev. E* **2004**, *69*, 041401.
(22) Nitta, T.; Endo, Y.; Haga, H.; Kawabata, K. *J. Electron Microsc.* **2003**, *52*, 277.
(23) Mohanty, B.; Aswal, V. K.; Kohlbrecher, Bohidar, H. B. *J. Polym. Sci.: Part B* **2006**, *44*, 1653.
(24) Geissler, E. In *Dynamic Light Scattering*; Brown, W., Ed.; Oxford: London, 1993.
(25) Coviello, T.; Geissler, E.; Meier, D. *Macromolecules* **1997**, *30*, 2008.
(26) Sharma, J.; Bohidar, H. B. *Colloid Polym. Sci.* **2000**, *278*, 15.
(27) Ren, S. Z.; Sorensen, C. M. *Phys. Rev. Lett.* **1993**, *70*, 1727.
(28) Viebke, V.; Piculell, L.; Nilsson, S. *Macromolecules* **1994**, *27*, 4160.
(29) Key, P. Y.; Sellen, D. B. *J. Polym. Sci.: Polym. Phys.* **1982**, *20*, 659.
(30) Dietler, G.; Cannel, D. S. *Phys. Rev. Lett.* **1988**, *60*, 1652.
(31) Corti, M.; Minero, M.; Degiorgio, V. *J. Phys. Chem.* **1989**, *88*, 309.
(32) Li. Y.; Tanaka, T. *J. Chem. Phys.* **1989**, *90*, 5161.
(33) Tokita, M.; Hikichi, K. *Phys. Rev. A* **1987**, *35*, 4329.
(34) Feng, S.; Sen, P. N. *Phys. Rev. Lett.* **1984**, *52*, 216.
(35) Nicolai, T.; Brown, W. *Light Scattering: Principles and Applications*; Clarendon: Oxford, 1996.
(36) Winter, H. H. *Polym. Eng. Sci.* **1987**, *7*, 1698.
(37) Labropoulos, K. C.; Niesz. D E.; Danforth. S. C.; Kevrekidis, P. G. *Carbohydr. Polym.* **2002**, *50*, 393 and ibid 407.
(38) Chen, Q.; Suki, B.; An, Kai-Nan *Trans. ASME* **2004**, *126*, 666.
(39) Normand, V.; Lootens, D. L.; Amici, E.; Plucknett, K. V.; Aymad, P. *Biomacromolecules* **2000**, *1*, 730.
(40) Eldridge, J. E.; Ferry. J. D. *J. Phys. Chem.* **1954**, *54*, 992.
(41) Watase, M.; Nishinari, K. *Rheol. Acta* **1983**, *22*, 580.
(42) Ajji, A.; Choplin, L. *Macromolecules* **1991**, *24*, 5221.
(43) Feke, G. T.; Prins, W. *Macromolcules* **1974**, *7*, 527.
(44) Altmann, N.; Cooper-White, J. J.; Dunstan, D. E.; Stokes. J. R. *J. Non-Newtonian Fluids* **2004**, *124*, 129.